POLITECNICO MILANO 1863

Department of Aerospace Science and Technology

Spacecraft Attitude Dynamics and Control (A.Y. 2022/23)

Final Project:

Attitude Determination and Control of a 3U CubeSat

Group 69:

Davide Lanza	10567211
Rocco Larocca	10660565
Matteo Mascelloni	10324919
Afaq Shakeel	10625777

Prof. Franco Bernelli Zazzera

Contents

List of Figures

List of Tables

Nomenclature

Symbol	Meaning	Unit of measurement
$\boldsymbol{B}$	Body reference frame	–
$\boldsymbol{r_{CG}}$	Center of gravity position	mm
J	Inertia matrix	$kg \cdot m^2$
J_{wheel}	Wheel inertia matrix	$kg \cdot m^2$
$\boldsymbol{I}$	Inertia vector	$kg \cdot m^2$
a	Orbit semi-major axis	km
e	Orbit eccentricity	–
i	Orbit inclination	rad
e	Orbit eccentricity	–
$\boldsymbol{r}$	Position vector in inertial frame	km
μ	Gravitational parameter	$\frac{km^3}{s^2}$
$\boldsymbol{b_N}$	Magnetic field in inertial frame	$\frac{A}{m}$
A_ϵ	Orthogonality error matrix	rad
$\boldsymbol{b_S}$	Measured magnetic field	$\frac{A}{m}$
$\boldsymbol{\omega_S}$	Measured angular velocity	$\frac{rad}{s}$
$\boldsymbol{\omega_B}$	Angular velocity in body frame	$\frac{rad}{s}$
$\boldsymbol{h_r}$	Reaction wheels angular momentum	$\frac{kg \cdot m^2}{s}$
A^*	Pseudo inverse matrix	–
$\boldsymbol{T_c}$	Control torque	Nm
$\boldsymbol{T_d}$	Disturbance torque	Nm
$A_{B/N}$	DCM-inertial to body	–
$A_{B/N_{est}}$	Estimated DCM-inertial to body	–
A_{obs}	Observed DCM	–
$A_{L/B}$	DCM-body to LVLH	–
G	Gain parameter	–
$[\omega\Lambda]$	Anti-symmetric matrix	$\frac{rad}{s}$
$\boldsymbol{\omega_{obs}}$	Observed angular velocity	$\frac{rad}{s}$
$\boldsymbol{\omega_{est}}$	Estimated angular velocity	$\frac{rad}{s}$
A_{err}	Pointing error matrix	–
$A_{L/N}$	DCM-inertial to LVLH	–
K_p	Proportional tuning parameters	–
K_d	Derivative tuning parameters	–
$\boldsymbol{\omega_L}$	Angular velocity in LVLH frame	$\frac{rad}{s}$

Acronyms

ARW	Angular Random Walk	FoV	Field of View
LVLH	Local Vertical Local Horizontal	DCM	Direction Cosine Matrix

1 Introduction

The main objective of this report is to provide a detailed analysis of the attitude determination and control systems for a 3U-CubeSat designed for Earth orbit. The goal is to maintain the payload pointing towards the Nadir with an accuracy of 1^o.
The report will cover all aspects of the attitude determination and control systems, including physical and mathematical considerations, as well as the assumptions and constraints involved. Real-world solutions available on the market are also discussed, taking into account the requirements of the customer and the constraints of the satellite's size and intended orbit.

1.1 Satellite Geometry

A 3U-CubeSat is a satellite with a length of 30 cm along one axis, where the factor $U = 10$ cm represents the form factor. As clarified by Fig.1.1, it has been chosen to extend the satellite along the x-axis in order to maintain the payload's instruments (red surface on the bottom) always pointing the Earth's surface on the -x-axis (Nadir) direction, while the solar panels (blue surfaces) have been positioned on top of the satellite, parallel to the y-axis.

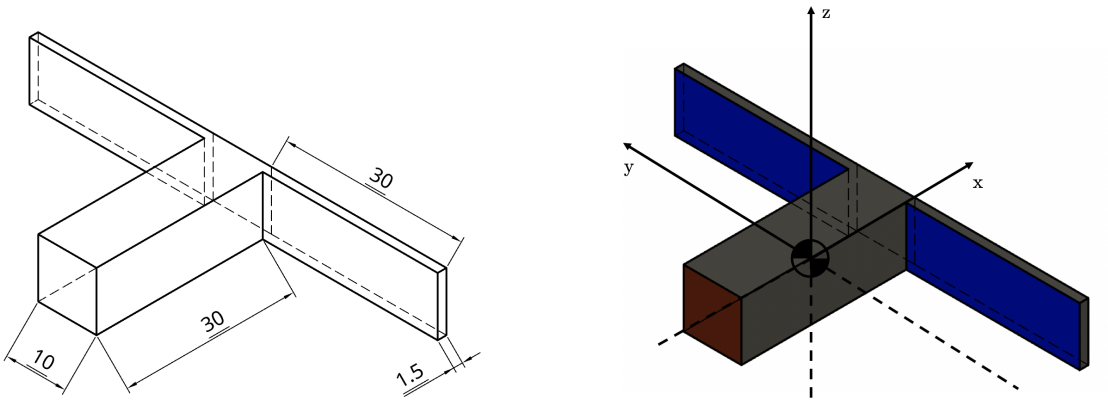

Figure 1.1: Satellite Geometry and Sizing

The reference frame **{x,y,z}** will be referred to as the body frame $\boldsymbol{B}$ and, for simplicity, its axes will be aligned with the principal axes of inertia of the spacecraft. The total mass of the spacecraft has been estimated to be 3.6 kg, with the majority of this weight coming from the solar panels which weigh 0.4 kg. As a result, the center of mass of the spacecraft is slightly shifted towards the top with respect to the barycenter of the CubeSat without solar panels.

$$\boldsymbol{r_{CG}} = \{0.132, 0, 0\}^T \text{ mm}$$

The mass and dimensions of the satellite, including the deployed solar panels, have been used to calculate the inertia matrix, which is given by:

$$J = \begin{bmatrix} 0.0124 & 0 & 0 \\ 0 & 0.0386 & 0 \\ 0 & 0 & 0.0373 \end{bmatrix} \text{ kg} \cdot \text{m}^2$$

1.2 Orbit Specifications

The orbit specifications have been chosen based on the goal of constantly pointing the Earth and to meet a customer requirement for an on-board Earth horizon sensor: indeed, as it will be discussed in more detail in Sec.2.3, this type of sensor must be close enough to the Earth's

surface to provide useful measurements. Consequently, a near-equatorial, near-circular Low-Earth Orbit (LEO) has been selected, with the following Keplerian coordinates being applied:

a [km]	e [-]	i [deg]	Ω [deg]	ω [deg]	θ [deg]
8000	0.01	0.028	30	0	0

Table 1: Initial Orbital Elements

1.3 On-Board Instrumentation

1.3.1 Sensors

- **Earth Horizon Sensor:**

The Earth Horizon Sensor selected for this project is the *CubeSense N 1st Gen.*, a highly accurate scanning instrument with a successful track record in space flight and low power consumption, manufactured by CubeSpace [1]. It has the following specifications:

FoV [deg]	$\pm$ 90
Rate [Hz]	2
Dimensions [mm]	41.7 x 17.7 x 22.9
Mass [g]	30
Accuracy [deg]	$<$0.2 (3σ)

Table 2: Earth Horizon Sensor Specifics

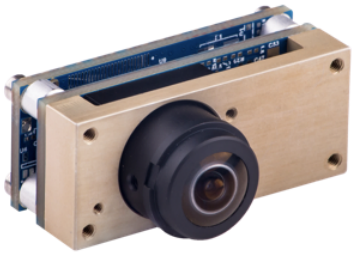

Figure 1.2: CubeSense N

As it will be explained in Sec.2.5.2, for the purpose of attitude determination, at least two different measurements are required.

- **Magnetometer:**

The chosen magnetometer for the attitude determination process is the *Spacemag-Lite* produced by Bartington [2]. This three-axis magnetometer has been selected due to its compatibility with the chosen orbit and the intensity of the Earth's magnetic field (see Sec.2.2). It is characterized by the following specifications:

Rate [Hz]	1
Saturation [μT]	$\pm$60
Noise [pT]	50
Dimensions [mm]	20 x 20 x 20
Mass [g]	67

Table 3: Magentometer Specifics

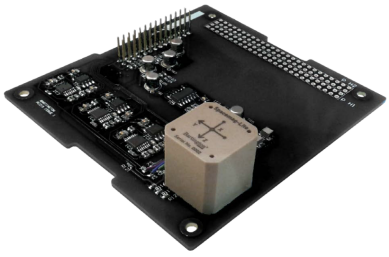

Figure 1.3: Spacemag-Lite

To ensure reliable attitude determination during all phases of the mission, especially during the initial stages after release from the launcher's capsule, a third sensor has been added in the form of a gyroscope. This, in combination with the Earth horizon sensor and magnetometer, should provide accurate attitude determination when the Earth is in the field of view of the former. Redundancy considerations have also played a role in the inclusion of the gyroscope.

- **Gyroscope:**

The *STIM300* produced by Sensonor [3] has been selected as the gyroscope for this project. This inertial measurement unit has demonstrated high performance, has a small size and low weight, and is relatively low cost. It is also immune to magnetic fields and has the following specifications:

Rate [samples/s]	2000
ARW $[^o/\sqrt{h}]$	0.15
Bias $[^o/h]$	0.3
Dimensions [mm]	39 x 45 x 25
Mass [g]	55

Table 4: Gyroscope Specifics

Figure 1.4: STIM300

1.3.2 Actuators

For the actuators' design, the choice has been fully driven by the customer's requirement of two reaction wheels and one inertia wheel as a minimum set-up. However, the number of reaction wheels has been increased for performance reasons (see Sec.2.4). The selected units are:

- **Reaction Wheels:**

Three *RL-RW-0.01* reaction wheels produced by RocketLab [4] have been selected as optimal for addressing the disturbance torques expected in the chosen orbit. Their specifications are:

Momentum [Nm·s]	$18 \cdot 10^{-3}$
Max. Torque [Nm]	0.001
Dimensions [mm]	50 x 50 x 30
Mass [g]	120

Table 5: Reaction Wheels Specifics

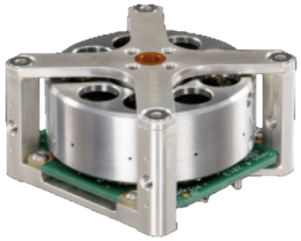

Figure 1.5: RL-RW-0.01

- **Inertia Wheel:**

The *CubeWheel Small CW0017* produced by CubeSpace [5] has been selected as the inertia wheel due to its compact size and high performance capabilities. Its specifications are:

Nominal Speed (Max) [rpm]	6000 (8000)
Radius [mm]	28
Height [mm]	26.2
Mass [g]	60

Table 6: Inertia Wheel Specifics

Figure 1.6: CW0017

2 Models Description

2.1 Spacecraft Dynamics and Kinematics

The analysis of the satellite's behavior as a rigid body orbiting in a dynamic field has involved decoupling orbital mechanics and attitude dynamics due to their significantly different time scales.
To compute the satellite's position vector along its orbit, a simple closed loop approach has been used, ignoring the effects of orbital perturbations and assuming a model without uncertainties. The integration of the CubeSat trajectory has been performed by solving the ordinary differential equation for the restricted two-body problem, taking into account the desired orbital characteristics.
The translational component between the inertial reference frame and the body principal axis frame has been neglected, and the modeling of the CubeSat's dynamical state has been accomplished using Euler's equations:

$$\boldsymbol{I} \cdot \dot{\boldsymbol{\omega}} = (\boldsymbol{I} \cdot \boldsymbol{\omega}) \times \boldsymbol{\omega} + \boldsymbol{T_c} + \boldsymbol{T_d} \tag{1}$$

where $\boldsymbol{I}$ is the inertia vector and $\boldsymbol{\omega}$ is the angular velocity of the CubeSat, both expressed in the body principal axes reference frame. As initial angular velocity vector, considering the perturbations given by the satellite's release by the launcher, it has been chosen to adopt:

$$\boldsymbol{w_B}(0) = [0.1, 0.1, 0.1] \text{ rad/s}$$

The control torque $\boldsymbol{T_c}$ applied through the actuators is necessary to maintain the desired attitude characteristics of the satellite throughout the mission. Additionally, the satellite's controllability must be able to prevent and counter any unwanted rotations caused by external disturbance torques ($\boldsymbol{T_d}$) through the correction of their overall effect.
On the other hand, in order to determine the kinematics of the system, an integration scheme based on the Direction Cosines Matrix (DCM, as requested by the customer) has been structured following the differential equation:

$$\frac{dA_{B/N}}{dt} = -\left[\omega\Lambda\right] A_{B/N} \tag{2}$$

The adopted initial $A_{B/N}(0)$ has been taken equal to a 3×3 identity matrix. Furthermore, to preserve its structure, it is necessary to orthonormalize the DCM at each integration step k by using an iterative scheme such as:

$$A_{k+1}(t) = \frac{3}{2}A_k(t) - \frac{1}{2}A_k(t) \cdot A_k(t)^T \cdot A_k(t) \tag{3}$$

2.2 Environment

The major disturbance torques acting on the spacecraft are selected in accordance with the given orbital parameters and altitude as shown in Figure 2.1.
This has led to consider Earth's gravity field and magnetic field as the most relevant sources of external disturbances.

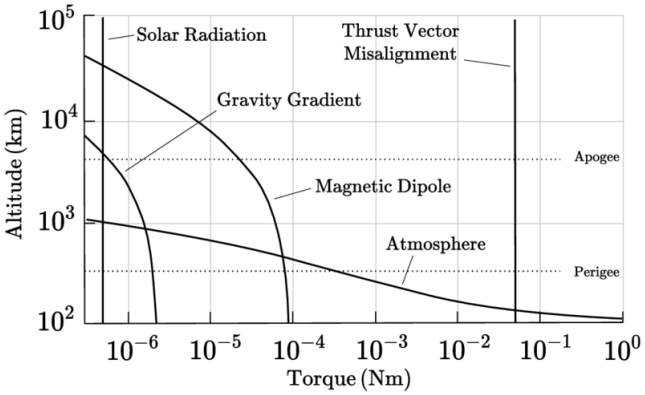

Figure 2.1: Relevance of Disturbance Torques Depending on the Altitude

2.2.1 Gravity Gradient

The non-uniformity of the Earth's gravity field results in a gravitational gradient torque acting on the satellite. This torque is the outcome of the difference in gravitational accelerations experienced by different parts of the satellite due to its mass distribution and orientation relative to the Earth. It can be estimated as:

$$\boldsymbol{M_{GG}} = \frac{3\mu}{|\boldsymbol{r}|^3} \begin{pmatrix} (I_z - I_y)c_2c_3 \\ (I_x - I_z)c_1c_3 \\ (I_y - I_x)c_2c_1 \end{pmatrix} \quad \text{with} \quad \begin{bmatrix} c_1 & c_2 & c_3 \end{bmatrix} = A_{B/L} \begin{bmatrix} 1 \\ 0 \\ 0 \end{bmatrix} \tag{4}$$

2.2.2 Magnetic Field

Interaction between Earth's magnetic field and the residual magnetic induction due to on-board currents within the electronic components can generate torques on the spacecraft. The magnetic field vector in inertial frame is then obtained as:

$$\boldsymbol{b_n} = \frac{{R_E}^3 \boldsymbol{H_0}}{|\boldsymbol{r}|^3}[3(\hat{\boldsymbol{m}} \cdot \hat{\boldsymbol{r}})\hat{\boldsymbol{r}} - \hat{\boldsymbol{m}}] \tag{5}$$

where R_E is the Earth's radius, H_0 is computed from the first order Gaussian coefficients of the IGRF (International Geomagnetic Reference Field), $\hat{r}$ is the versor in the direction of $\boldsymbol{r}$, and $\hat{m}$ is the direction of the magnetic field. The latter versor has been computed as follows:

$$\hat{\boldsymbol{m}} = \begin{pmatrix} sin(11.5^o)cos(\omega_E t) \\ sin(11.5^o)sin(\omega_E t) \\ cos(11.5^o) \end{pmatrix} \tag{6}$$

where ω_E is the Earth's angular velocity about its axis of rotation. The torque has been then finally modeled:

$$\boldsymbol{T_{mag}} = \boldsymbol{m} \times (A_{B/N}\boldsymbol{b_N}) = \boldsymbol{m} \times \boldsymbol{b_B} \tag{7}$$

where $\boldsymbol{m} = [0.01, 0.05, 0.1]^T \ \frac{A}{m^2}$ is the residual dipole of the satellite.

2.3 Sensors

Attitude determination and control require accurate data from on-board sensors, which are essential for the proper functioning of a satellite. To simulate the attitude of the spacecraft, a model of each sensor must be developed, taking into account the most significant errors and noise that may affect their measurements. As mentioned in Sec. 1.3, three sensors have been

selected for the 3U-CubeSat under development: an Earth horizon sensor, a magnetometer, and a gyroscope.
In this section, an overview of the mathematical models on which these sensors are based will be provided, discussing the potential sources of measurement disturbance for each.

2.3.1 Earth Horizon Sensor

The Earth horizon sensor is mounted on the same face of the satellite as the payload's instruments, and is ideally pointing directly towards the Nadir direction. However, this condition is only guaranteed during the later stages of the mission. Therefore, a dedicated block has been implemented to determine if the sensor's scanning lens is actually pointing towards the Earth, or in other words, if the Earth is within the sensor's field of view (FoV). To do this, the position vector has been computed as in Sec.2.1 and rotated from the inertial frame to the body frame using the $A_{B/N}$ matrix. The angle between $\boldsymbol{r_B}$ and the versor $\hat{\boldsymbol{x}}$ =[-1,0,0]^T, which indicates the Nadir direction, has been then calculated. If the result was larger than the sensor's FoV, it was determined that the horizon sensor was not effectively pointing towards the Earth and would not function properly. If the condition was satisfied, the horizon sensor was available for measurements and the estimated position vector's direction $\boldsymbol{r_S}$ could be retrieved. Furthermore, the errors introduced by the sensor have been modeled by generating three random errors $[\alpha_x, \alpha_y, \alpha_z]$ within a specified range and distribution based on the sensor's accuracy and the instrument's sampling time (see Tab.2). These errors have been then filtered by a factor of 10 and shaped into a small rotation matrix A_ε such that:

$$\overline{\boldsymbol{r_S}} = A_\varepsilon \boldsymbol{r_S}, \quad \text{where } A_\varepsilon = \begin{bmatrix} 1 & \alpha_z & -\alpha_y \\ -\alpha_z & 1 & \alpha_x \\ \alpha_y & -\alpha_x & 1 \end{bmatrix} \tag{8}$$

In order to prevent the error matrix from changing too rapidly, the value of the signal has been held for a specific period of time before being allowed to change again. This approach allows the error matrix to be updated at a slower rate than the simulation's sampling time.

2.3.2 Magnetometer

Previously, it has been explained that the Earth horizon sensor only provides information about the satellite's orientation in two dimensions (pitch and yaw). To complete the attitude determination process, a second sensor is required. The chosen additional sensor for this purpose is the magnetometer, which provides stable and accurate readings in the region in which the satellite is operating, which is approximately normal to the Earth's magnetic field.
The role of the magnetometer is to measure the vector of the magnetic field, designated as $\boldsymbol{b_S}$, and compare it to the modeled magnetic field vector in the body frame, referred to as $\boldsymbol{b_N}$. From this comparison, the magnetometer can provide information about the attitude of the spacecraft. In this process, it is necessary to take into account two sources of disturbance:

- Non-linearities, which are represented by the vector $\boldsymbol{c(b_N)}$, and are also associated with the magnetometer's noise due to hysteresis (as shown in Table 3), that are taken into account in the rotation from the inertial to the body reference frame;
- Systematic errors, simulated as random numbers that make up an error matrix A_ε.

The combination of these contributions yields:

$$\boldsymbol{b_S} = \boldsymbol{c(b_N)} A_\varepsilon \boldsymbol{b_N} \tag{9}$$

Additionally, saturation limits are imposed to prevent instability in the simulation in the event of large error values.

2.3.3 Gyroscope

In Sec.1.3, it has been described how the chosen attitude determination process becomes inactive if the Earth horizon sensor does not see the Earth in its FoV (see Sec.2.5): this situation can be very frequent during detumbling in which the satellite, when released by the launcher's capsule, does not have a refined attitude control. Therefore, despite being able to function properly on its own under normal conditions, an additional sensor that is independent of external sources has been added and identified as the gyroscope.
For the mathematical modelling of the gyroscope, its output $\boldsymbol{w_S}$ has been considered as the result of the comparison between the measured and the real $\boldsymbol{w_B}$. Consequently, following a similar discussion to the one done for the magnetometer, non-linearity terms as well as white noises have been taken into account as follows:

$$\boldsymbol{w_S} = \boldsymbol{w_B} + \boldsymbol{n} + \boldsymbol{b} \tag{10}$$

In particular, $\boldsymbol{n}$ represents a white noise based on the ARW of the gyroscope, while $\boldsymbol{b}$ represents the integrated bias term (data are available in Tab.4).

2.4 Actuators

The selected actuators for the satellite are three reaction wheels and one inertia wheel, activated after detumbling. The chosen configuration imposes the three reaction wheels along each one of the principal axes and one inertia wheel along the major spinning z-axis: this way, a precise and independent control of the satellite's attitude is obtained in all the phases of the mission.

2.4.1 Reaction Wheels

The three reaction wheels are used among the entire mission as implementation of the control's algorithms output: indeed, they are directly commanded by the controller of the satellite and act by absorbing or releasing angular momentum within the spacecraft. The provided angular momentum variation can be expressed as:

$$\dot{\boldsymbol{h}}_{\boldsymbol{r}} = -A^*(\boldsymbol{T_c} + \boldsymbol{\omega} \times A\boldsymbol{h_r}) \tag{11}$$

where A and A* are connected to the orientation of the reaction wheels, while $\boldsymbol{T_c}$ is coming as an input from the controller.
Being the reaction wheels three electric motors, typical operational curves can be retrieved, and consequently precise boundaries in the applicable momenti. This condition has been translated in a selector algorithm giving a zero contribution whenever the momentum value indicated in Tab.5 is overlapped. At the same time, considering the nature of the spinning rotor embedded in the reaction wheels, a maximum possible torque must be established between two symmetric saturation values.

2.4.2 Inertia Wheel

The inertia wheel has the role of refining the spacecraft's stability: due to its nature, it results to work better for low values of torques so, as anticipated, it has been decided to activate it only after detumbling, then leaving it to passively spin for the rest of the mission.
The angular momentum of the inertia wheel has been calculated through a product between its characteristic inertia matrix (obtained by its geometry and mass values) and its angular velocity vector retrieved by the nominal speed per minute (see Tab.6):

$$\boldsymbol{h_r} = J_{wheel}\boldsymbol{w_r} \tag{12}$$

The result has been then directly applied to the spacecraft's dynamics block, being added to the effective $\boldsymbol{h_B}$.

2.5 Attitude Determination

2.5.1 Attitude Determination Algorithm

Attitude determination is the process of estimating the orientation of a spacecraft relative to a reference frame. It is important to precisely model the attitude determination process to ensure that it provides reliable and accurate estimates of the spacecraft's orientation. The algebraic method has been chosen to model this block. One key benefit is the ability to accurately estimate the spacecraft's orientation using a mathematical model of the system's dynamics and sensor fusion techniques. This approach results to be particularly useful for the purposes of this report as it allows to account for external influences such as the gravity gradient and the Earth's magnetic field. Another advantage is its flexibility in handling various sensor configurations, which is important due to the use of multiple types of sensors. Additionally, this method is computationally efficient, making it suitable for low-power systems, and is effective at handling discrepancies between sensor measurements and accounting for uncertainty in sensor data.
In nominal conditions two orthogonal frames, **s** and **v**, are built as follows:

$$\begin{cases} \boldsymbol{s}_1 = \boldsymbol{p} \\ \boldsymbol{s}_2 = \frac{\boldsymbol{p}\times\boldsymbol{q}}{|\boldsymbol{p}\times\boldsymbol{q}|} \\ \boldsymbol{s}_3 = \boldsymbol{p}\times\boldsymbol{s}_2 \end{cases} , \quad \begin{cases} \boldsymbol{v}_1 = \boldsymbol{a} \\ \boldsymbol{v}_2 = \frac{\boldsymbol{a}\times\boldsymbol{b}}{|\boldsymbol{a}\times\boldsymbol{b}|} \\ \boldsymbol{v}_3 = \boldsymbol{a}\times\boldsymbol{v}_2 \end{cases} \tag{13}$$

where $\boldsymbol{p}$ and $\boldsymbol{q}$ are the measurements in the body frame while $\boldsymbol{a}$ and $\boldsymbol{b}$ their corresponding directions in the inertial reference system. Finally, the estimated DCM can be built:

$$A_{B/N_{est}} = SV^T \tag{14}$$

where S and V are the matrices formed by the retrieved orthogonal vectors.
In non-nominal conditions, when the Earth is out of the horizon sensor's FoV, the angular velocity measurements coming from the gyroscope are used to propagate the attitude through the integration of the following differential equations:

$$\frac{dA_{B/N}}{dt} = \begin{bmatrix} 0 & \omega_z & -\omega_y \\ -\omega_z & 0 & \omega_x \\ \omega_y & -\omega_x & 0 \end{bmatrix} A_{B/N} \tag{15}$$

The A matrix is then orthonormalized at each step to preserve its orthogonality properties.

2.5.2 State Observer

To maintain the accuracy of the data, it is necessary to mitigate the effects of noise in the gyroscope output and in the estimated attitude. While a low-pass filter could be used for this purpose, it is not practical for real-time processing due to the potential for significant phase delay. As an alternative, a state observer has been implemented to filter the data without introducing any delay. The observer's behavior is based on the same equation that governs the kinematics in terms of DCM.

$$\begin{cases} \frac{dA_{obs}}{dt} = [-\omega\Lambda]A_{obs} + G_1(A_{est} - A_{obs}) \\ I\frac{d\boldsymbol{\omega_{obs}}}{dt} = I\boldsymbol{\omega_{obs}}\times\boldsymbol{\omega_{obs}} + \boldsymbol{T_d} + \boldsymbol{T_c} + G_2(\boldsymbol{\omega_{obs}} - \boldsymbol{\omega_{est}}) \end{cases} \tag{16}$$

The matrix $[\omega\Lambda]$ is composed of the elements of the vector $\boldsymbol{\omega_{obs}}$, coming from a prior refinement of the gyroscope's output. The value of the gain parameters G_i significantly impact the performance of the observer, influencing both convergence rate and robustness to noise and disturbances. The optimal values of G_i depend on the system being observed and the desired performance of the observer. For instance, a larger values of G_i may lead to faster convergence,

but may also increase sensitivity to noise and disturbances. On the other hand, smaller values of G_i may offer improved robustness, but may also result in slower convergence. For this application, the values -0.6 (for the DCM loop) and -0.5 (for the angular velocity loop) have been chosen to achieve an appropriate balance between convergence rate and robustness.

2.6 Control Algorithms

The controller block calculates control inputs to drive the system towards a desired state obtained by a feedback from the system itself. In this project, three different mission phases are required: detumbling for the first 300 seconds to stabilize the initial attitude, a slew maneuver to reach the desired orientation, and pointing to maintain orientation towards the Earth for the remainder of the mission. Consequently, the controller block must adapt to these phases and maintain system performance, guaranteeing also the stability of the system.

2.6.1 Detumbling

During the detumbling phase of the mission, a linear controller has been implemented to stabilize the orientation of the spacecraft. The controller uses an input of the angular velocity of the spacecraft, and generates control inputs in the form of torques to be applied by the spacecraft's reaction wheels, as follows:

$$\boldsymbol{T_c} = -K\boldsymbol{\omega_{obs}} \tag{17}$$

where $\boldsymbol{T_c}$ is the applied torque, K is a constant gain term, and $\boldsymbol{\omega}_{obs}$ is the angular velocity of the spacecraft coming from the state observer block. The gain value has been chosen as 0.001, based on the desired convergence rate and robustness to noise and disturbances. This linear controller effectively drives the system towards a stable orientation, overcoming the effects of external disturbances. The simplicity and low computational cost of this linear controller make it an effective solution for the initial stabilization of the system.

2.6.2 Slew Maneuver & Earth Pointing

To maintain precise control over the satellite's orientation during the slew maneuver and Earth pointing phases, a non-linear controller has been implemented. This controller accurately tracks the desired orientation and maintains it for the duration of these phases. To point the satellite towards the Earth, the body frame must be aligned with the LVLH frame, with the orientation difference between the two determining the pointing error. To achieve a stable equilibrium configuration, it is necessary for one of the satellite's principal axes of inertia to be pointed towards the Earth. Therefore, the pointing error matrix to be controlled results to be:

$$A_{err} = A_{B/N} = A_{B/N}A_{L/N}^T \tag{18}$$

which has to be as close as possible to the identity matrix.
The control equations are comprised of a proportional and a derivative term, as follows:

$$\boldsymbol{T_c} = -\boldsymbol{K_p}(A_{err}^T - A_{err}) - \boldsymbol{K_d}(\boldsymbol{\omega_B} - \boldsymbol{\omega_L}) \tag{19}$$

where $\boldsymbol{\omega_B}$ and $\boldsymbol{\omega_L}$ represent the angular velocities in the body and LVLH reference frames, $\boldsymbol{K_p}$ and $\boldsymbol{K_d}$ are respectively the proportional and derivative tuning parameters. $K_{p,i}$ has been set to $3\cdot10^{-4}$, while $K_{d,i}$ to 10^{-2}. These values have been chosen based on the specific requirements and characteristics of the system. The proportional term is responsible for correcting the error between the current state and the desired state, while the derivative term helps to dampen oscillations and to improve the overall stability of the control system. The chosen values provide an appropriate balance between performance and stability, ensuring that the satellite is able to accurately track the desired orientation during the slew maneuver and Earth pointing phases.

2.7 Framework Overview

A MATLAB Simulink© code has been built for the entire simulation, assembling all the analyzed components following the mathematical models described above. The overall mission loop is qualitatively represented by Fig.2.2.

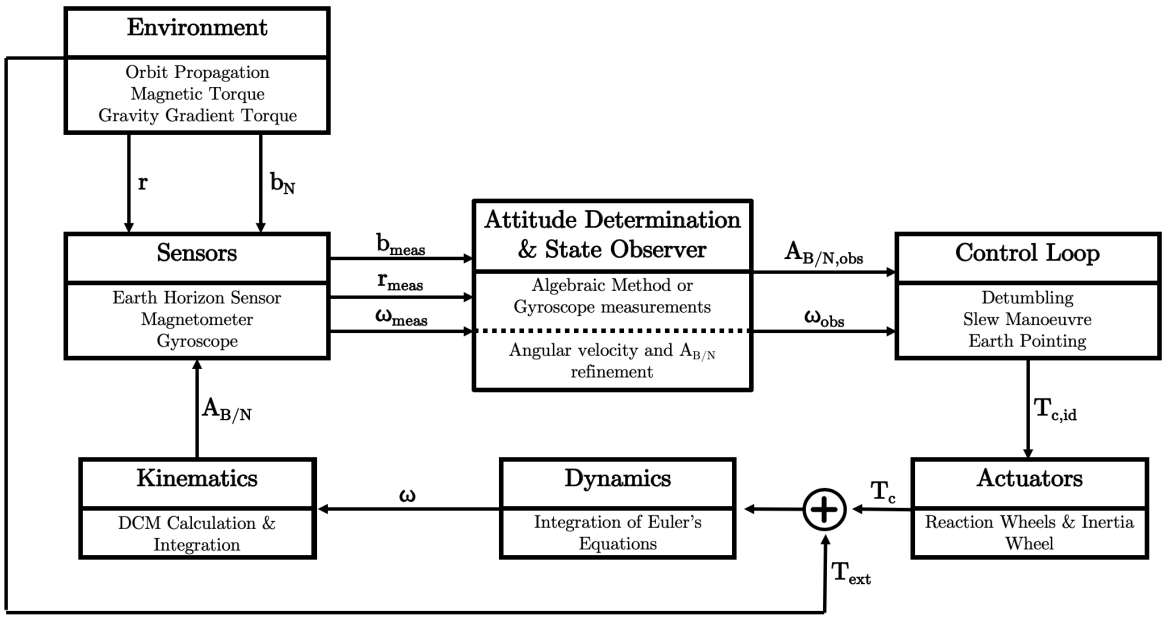

Figure 2.2: Attitude Determination and Control Loop

3 Results

The attitude determination and control systems on-board the 3U-CubeSat have been evaluated for a total of one full period, approximately equal to 1 h 58 min 41 s. Over this entire period, all the phases anticipated in Sec.2.6 are operated and fulfilled, finally satisfying the main requirement to point directly the Nadir with an accuracy of 1^o.

3.1 Uncontrolled Case

To give an entire overview on the initial state of the satellite and for a better interpreting of the next results, in this section a simulation of the uncontrolled case is shown and discussed. Having an uncontrolled spacecraft means to shut down all the instruments on-board, starting from the sensors, and letting the external environment propagate its effects on the satellite's attitude.
It can be noted how the angular velocities, starting from the initial values stated in Sec.2.1, propagate themselves reaching their maximum and minimum peaks around the values of ± 0.15 rad/s: in particular, the ω_z component appears to be the more problematic from this point of view, while the ω_x seems to be enough stabilized around the nominal value of 0.1. On the right side of Fig.3.1 a simulation of the external disturbances acting on an uncontrolled satellite dynamics has been carried out: the obtained trend results to be in agreement with the discussion developed in Sec.2.2, underlining the importance of the magnetic and gravity gradient disturbances.

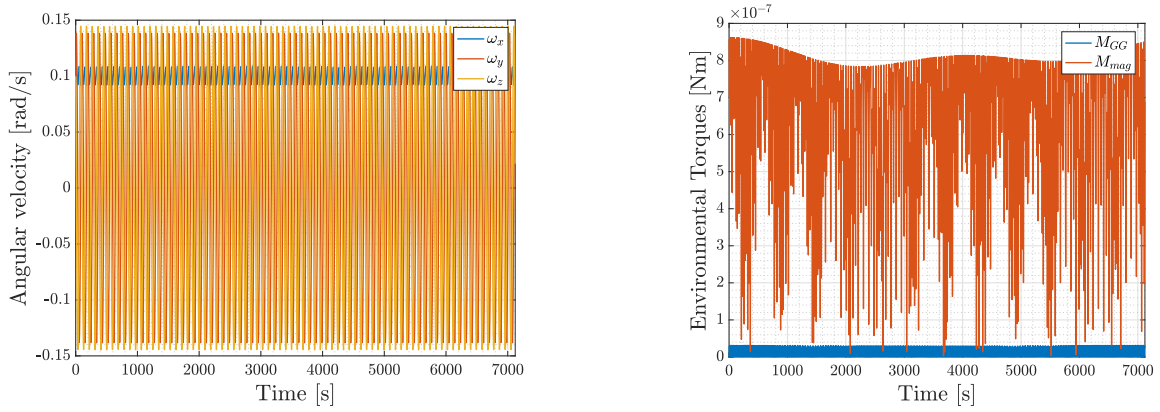

Figure 3.1: Angular Velocities and Disturbance Torques Evolution in the Uncontrolled Case

3.2 Controlled Case

The controlled case consists of all the three phases carrying the CubeSat to the mission objective of Earth's pointing. All these phases will be analyzed in terms of dynamics and control, evaluating not only the most practical results from the attitude point of view but also the performances of the embedded control and determination subsystems.

3.2.1 Detumbling

Detumbling covers the first 300 s of the mission, after which convergence is achieved: its purpose is to filter out all the initial disturbances resulting from the capsule release, allowing all the satellite's systems to power-up and to start working nominally.

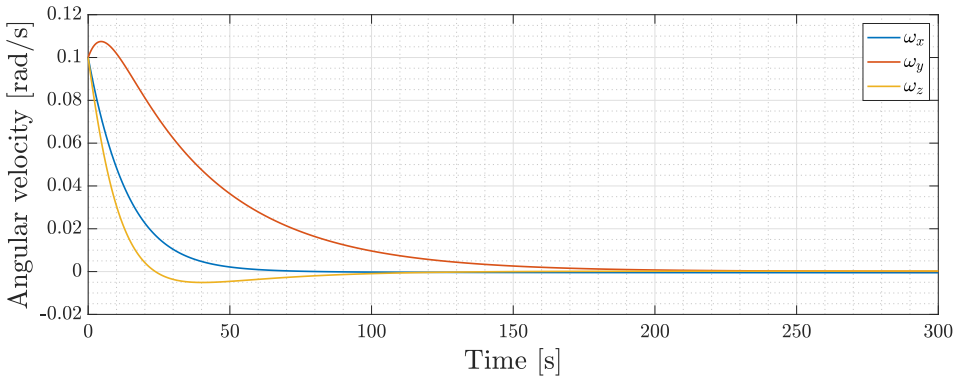

Figure 3.2: Angular Velocities during Detumbling Phase

As it can be appreciated in Fig.3.2, the angular velocities rapidly converge to zero thanks to the immediate action of the gyroscope and of the three reaction wheels respectively for the attitude determination and control.
The applied torques (Fig.3.3) follow a similar trend, immediately adjusting the attitude of the satellite after the capsule's release and ending the detumbling phase with an approximately zero-value.
From the performance point of view, evaluating the difference between the desired attitude matrix and the estimated one (Fig.3.4), high errors are expected during the first instants of detumbling since the three sensors are not immediately set-up and in a nominal condition. After approximately half time, the errors decrease to acceptable values.

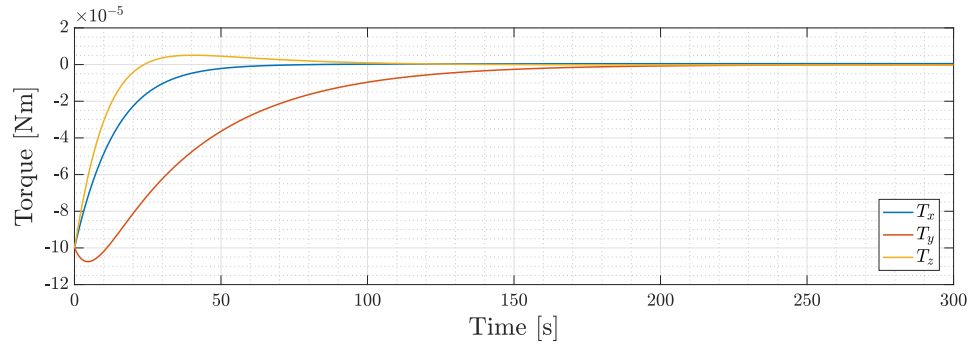

Figure 3.3: Applied Torques during Detumbling Phase

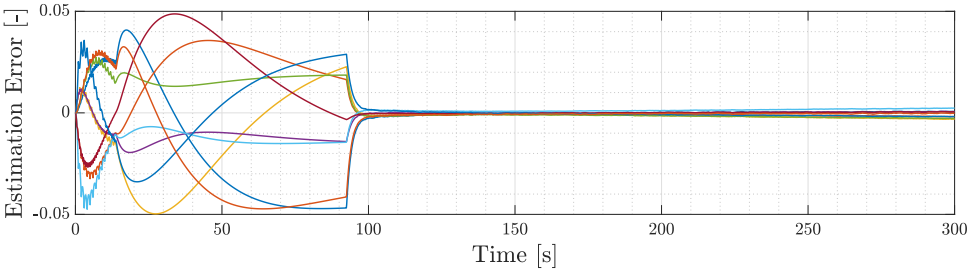

Figure 3.4: Estimation Error during Detumbling Phase

No pointing performances are provided during this phase since only after the slew maneuver the satellite will effectively start to accomplish the mission's objective.

3.2.2 Slew Maneuver

The slew maneuver begins at the end of detumbling with the aim of orienting the satellite to constantly point towards the Earth: high torques are expected as well as new peaks of angular velocities before reaching the final attitude conditions. The time fixed for the slew maneuver is about 900 s to assure and to test the nominal pointing condition, even though, as visible from Fig.3.5, a very good stability is reached already after 200 s.

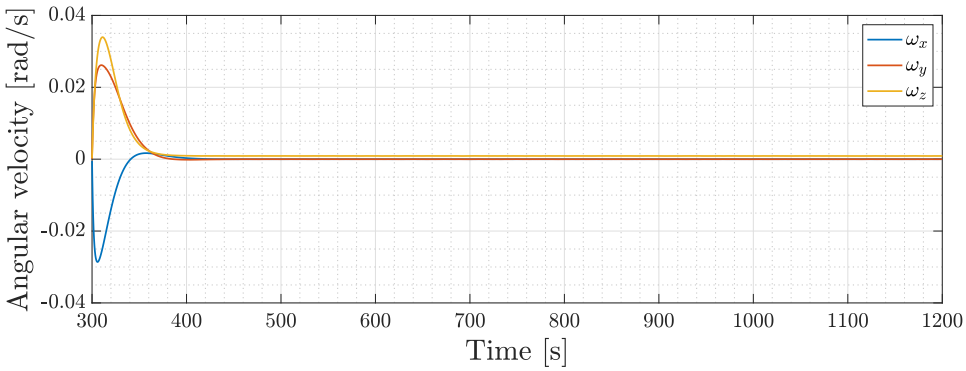

Figure 3.5: Angular Velocities during Slew Maneuver Phase

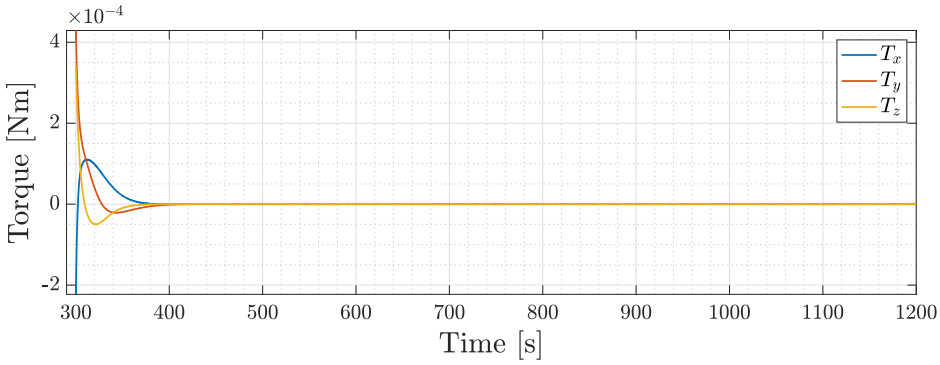

Figure 3.6: Applied Torques during Slew Maneuver Phase

Also in this case, the performance of the overall system has been verified through the error between desired and estimated attitude matrix. In the figure below, it is evident how these errors have decreased with respect to the detumbling phase and how they acquire, after a first peak, an oscillating behaviour around the zero value.

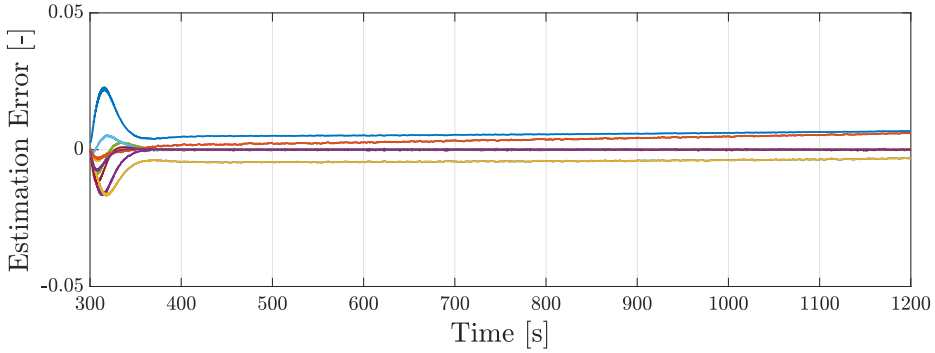

Figure 3.7: Estimation Error during Slew Maneuver Phase

For the slew maneuver it is also important to start evaluating the pointing performance looking at the error with respect to the assigned requirement.

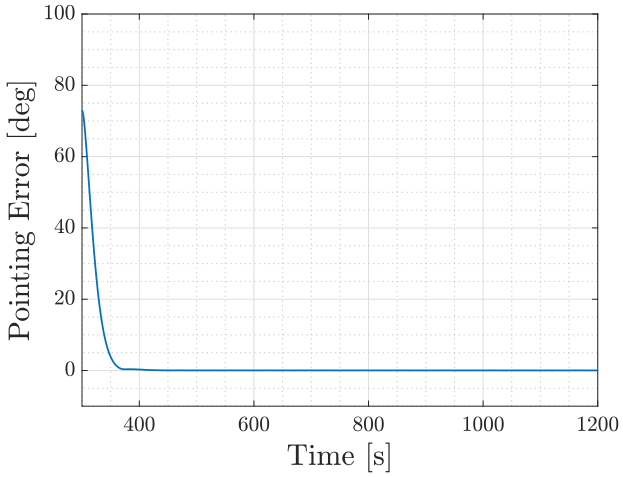

Figure 3.8: Pointing Accuracy during Slew Maneuver Phase

A precise pointing is assured after a very short time during the slew maneuver, justifying the sensors' nominal behaviour and manifesting the success of the attitude determination and control algorithms.

3.2.3 Earth's Pointing

The performance reached during the slew maneuver is reflected in the final phase of the mission which is the Earth's pointing. All the quantities begin to exhibit very small oscillating behaviors within certain limits, indicating a continuous interaction between the attitude determination and the corresponding control even for small rotations.

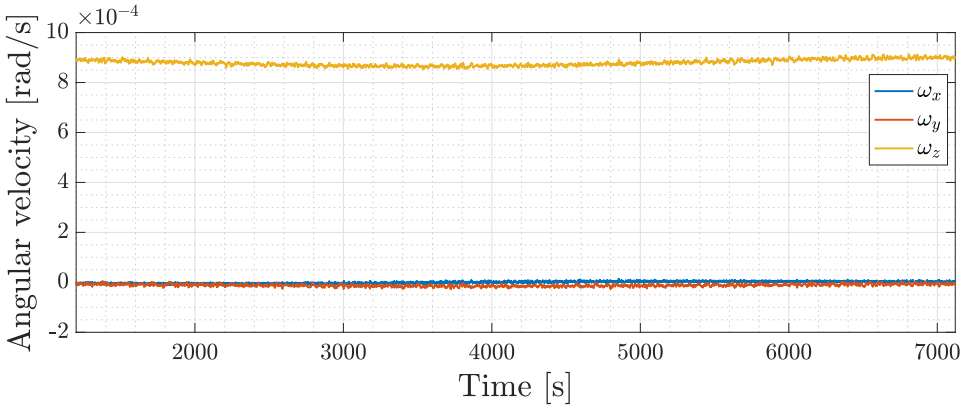

Figure 3.9: Angular Velocities during Pointing Phase

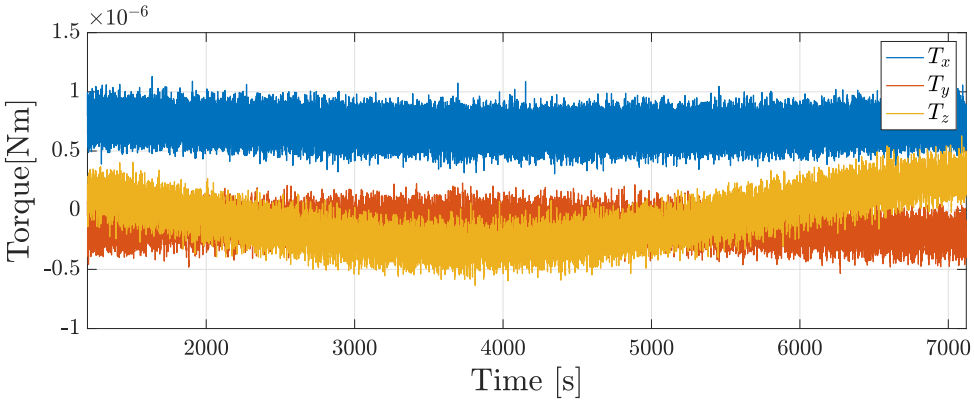

Figure 3.10: Applied Torques during Pointing Phase

Finally, the pointing error is taken to very small values and, as evident from Fig.3.11, also the external disturbances along all the mission are correctly counteracted and controlled.

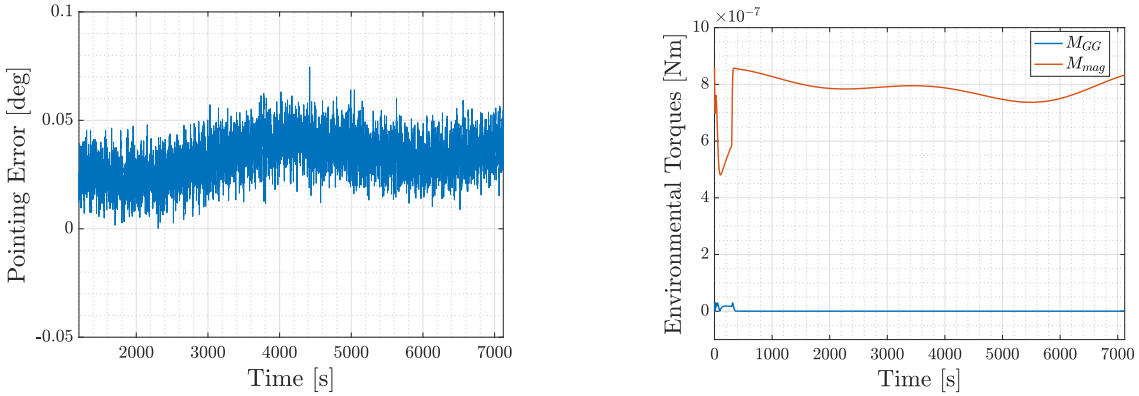

Figure 3.11: Pointing Accuracy during Pointing Phase and Disturbance Torques among the Mission

4 Final Considerations

The attitude dynamics control system developed in this project has demonstrated its effectiveness in controlling the orientation of the satellite to fulfill the detumbling and Earth pointing requirements. The implemented control laws, which include a proportional controller for the detumbling phase and a combination of proportional and derivative control for the Earth pointing phase, show stability and resistance to disturbances even when sensor readings are noisy.

While the values of the gain parameters have been determined through a trial and error method, future designs could utilize more advanced techniques to optimize these values. The model also accounts for the main dynamics and perturbations of the system, but could be refined with a more realistic magnetic model and with the implementation of solar radiation pressure disturbance, taking into account the possible movements of the solar panels based on sunlight exposure. Additionally, further analyses could be conducted to include a redundant reaction wheel, a mechanism for desaturation during high torque demands, or a more detailed study of the satellite's structure to achieve a more precise inertia matrix.

Overall, the performance of the attitude determination and control system in this project suggests its suitability for controlling the orientation of a small satellite such as a 3U-CubeSat, and its potential for improvement through further considerations and optimizations.

References

[1] CubeSpace, URL: `https://www.cubespace.co.za/products/gen-1/sensors/cubesense/`, consulted Dec. 2022

[2] Bartington, URL: `https://gmw.com/wp-content/uploads/2019/02/Spacemag-Lite_DS2714.pdf`, consulted Dec. 2022

[3] Sensonor, URL: `https://www.sensonor.com/products/inertial-measurement-units/stim300/`, consulted Dec. 2022

[4] Rocket Lab, URL: `https://www.rocketlabusa.com/assets/Uploads/RL-RW-0.01-Data-Sheet.pdf`, consulted Dec. 2022

[5] CubeSpace, URL: `https://www.cubespace.co.za/products/gen-2/actuators/cubewheel/`, consulted Dec. 2022

[6] J. Wertz, *Spacecraft Attitude Determination and Control*, D.Reidel

[7] F. Landis Markley, J. L. Crassidis, *Fundamentals of Spacecraft Attitude Determination and Control*, Springer

[8] F. Bernelli. Lecture notes of the course *Spacecraft Attitude Dynamics and Control*.

[9] C. Colombo. Lecture notes of the course *Orbital mechanics*.